ISSN 0022-4766, Journal of Structural Chemistry, 2023, Vol. 64, No. 8, pp. 1391-1398. © Pleiades Publishing, Ltd., 2023.
Russian Text © The Author(s), 2023, published in Zhurnal Strukturnoi Khimii, 2023, Vol. 64, No. 8, 113998.

ELECTRON DELOCALIZATION AND RELATIVISTIC EFFECTS IN THE ELECTRONIC STRUCTURE AND NMR PARAMETERS OF $[Cp^*_3M_3Se_2]^{2+}$ (*M* = Rh, Ir) COMPLEX CATIONS*

I. V. Mirzaeva[1]**

The question about the presence or absence of metal–metal bonds in $[Cp^*_3M_3Se_2]^{2+}$ complex cations, where *M* = Rh, Ir, is considered by density functional theory (DFT) methods. The bonding is analyzed by AIM, Foster–Boys localized orbitals, and NBO methods. It is shown that in these systems, due to the strong electron delocalization, it is better to speak about three-center *M*–*M*–Se and four-center *M*–Se–*M*–Se bonds rather than two-center metal–metal bonds. The compositions of bond orbitals differ in rhodium and iridium complexes. The analysis of contributions of different NBOs to the magnetic shielding of Se reveals that the difference in ^{77}Se NMR chemical shifts is related to a change in the contribution of the Se lone pair, antibonding *M*–Se orbitals, and an admixture of orbitals of the second Se atom in the iridium complex rather than the presence or absence of metal–metal bonds.

DOI: 10.1134/S0022476623080048

Keywords: ^{77}Se NMR, DFT, NBO, AIM, metal–metal bonds.

INTRODUCTION

NMR spectroscopy has been widely used to determine the molecular and electronic structures of organic compounds. However, when studying inorganic compounds, especially transition metal compounds, difficulties arise in the interpretation of results due to the strong electron delocalization and relativistic effects causing large ranges of possible chemical shifts and hardly predictable shifts of NMR signals [1]. The fundamental comprehension of relativistic and electron delocalization effects on NMR parameters can help with the search for NMR signals in new compounds and to obtain more information from experimental spectra. In this work, by the example of two similar chalcogenide Rh and Ir complex cations we demonstrate how the topological analysis of electronic structures and the analysis of localized orbitals can help explain NMR parameters and reveal the above-mentioned effects.

The $[Cp^*_3M_3Se_2]^{2+}$ (*M* = Rh, Ir) cations are of interest because these rhodium and iridium complexes have almost identical geometries but different spectroscopic properties [2, 3]. In particular, ^{77}Se NMR chemic shifts (CSs) are greatly

[1]Nikolaev Institute of Inorganic Chemistry, Siberian Branch, Russian Academy of Sciences, Novosibirsk, Russia; **dairdre@gmail.com. Original article submitted May 9, 2023; revised May 23, 2023; accepted May 24, 2023.

* Supplementary materials for this article are available at doi 10.1134/S0022476623080048 and are accessible for authorized users.

different. The question arises whether this is associated with the difference in electronic structures of the cations or not. If so, why different electronic structures do not result in different geometries of the cations? The previous analysis of chemical bonds in this pair of cations was carried out within Bader's atoms in molecules (AIM) theory [4]. The results showed that metal–metal bonds were not observed in the rhodium complex, and when heavier Ir substituted for Rh, these bonds appeared. However, calculations were performed with the use of only one functional (BP [5, 6]). It is interesting to check whether the absence or presence of metal–metal bonds depends on the functional or not and to compare the results with the bond pattern from other methods analyzing the electronic structure.

Principally another approach (in comparison with the topological methods such as AIM) is proposed by localized orbital analysis methods. One of them, namely the Boys–Foster orbital localization [7], can find and characterize metal–metal bonds in transition metal complexes [8]. Another popular method - the natural bond orbital (NBO) analysis [9] - often does distinguish metal–metal or metal–ligand bonds, classifying them as strongly delocalized lone pairs on either metal or ligand. However, NBO makes it possible to decompose the NMR shielding into contributions from different elements of the electronic structure. The method was proposed in [10] and then adapted to relativistic two-component calculations of NMR parameters [11].

The aim of this work was to study the presence or absence of metal–metal bonds in $[Cp^*_3M_3Se_2]^{2+}$ (M = Rh, Ir) cations using the AIM data with respect to different exchange-correlation functionals, the comparative analysis of electronic structures of these cations by Boys–Foster localized orbitals and NBO methods, and the explanation of observed differences in ^{77}Se NMR shifts of the mentioned cations.

COMPUTATIONAL METHODS

All calculations were performed using the ADF2017 program package [12] with Slater orbital basis sets [13]. Relativistic effects were taken into account by the zeroth order regular approximation (ZORA) [14]. Only scalar relativistic effects were taken into account in the geometry optimization and the electronic structure analysis. Spin-orbit relativistic effects were also taken into account in the calculation of NMR parameters by the gauge including atomic orbital (GIAO) method [15] and in their analysis. ^{13}C and ^{1}H NMR shifts were calculated relative to tetramethylsilane and ^{77}Se NMR shiftsrelative to selenium dimethyl. Tetramethylsilane and selenium dimethyl were pre-optimized with the same parameters as the main complexes.

RESULTS AND DISCUSSION

Geometry of the cations was optimized with several different pure functionals (OPBE [16], BP [4, 5], BLYP [4, 17]), including those taking into account dispersion corrections (S12g [18], PBE-D3(BJ) [19], and BP-D3(BJ) [19]). The obtained optimized *M–M* distances vary from 2.860 Å to 3.007 Å for Ir and from 2.843 Å to 2.998 Å for Rh (Tables S1 and S2, Supplementary Materials). If dispersion corrections are applied, shorter distances are obtained, which better correspond to the experimental data (depending on the counterion, 2.849-2.890 Å for M = Ir [3] and 2.880-2.888 Å for M = Rh [2]). The system is not symmetric relative to the *M–M–M* plane. The difference between average Se–*M* distances for Se atoms on different sides of the *M–M–M* plane ranges from 0.003 Å to 0.006 Å.

Dependence of the AIM results on the exchange-correlation functional. In iridium complexes, the presence or absence of Ir–Ir bond critical points (bcp) depends on the respective distance: if as a result of the geometry optimization, the distance is larger than 2.900 Å, then bcp is absent (OPBE, S12g, BP, BLYP functionals) and if it is shorter, then it is present (PBE-D3(BJ) and BP-D3(BJ) functionals). In the rhodium complex, Rh–Rh bcp are not observed in any case (Fig. 1).

Ring critical points inside Cp* and the corresponding cage points (local density minima) inside the Cp*–Ir pyramid are absent in the iridium complex for the PBE-D3(BJ) functional, which was not observed previously for calculations with the BP functional [3]. These points are present for Rh, but they are located too close to each other, i.e., they are close to

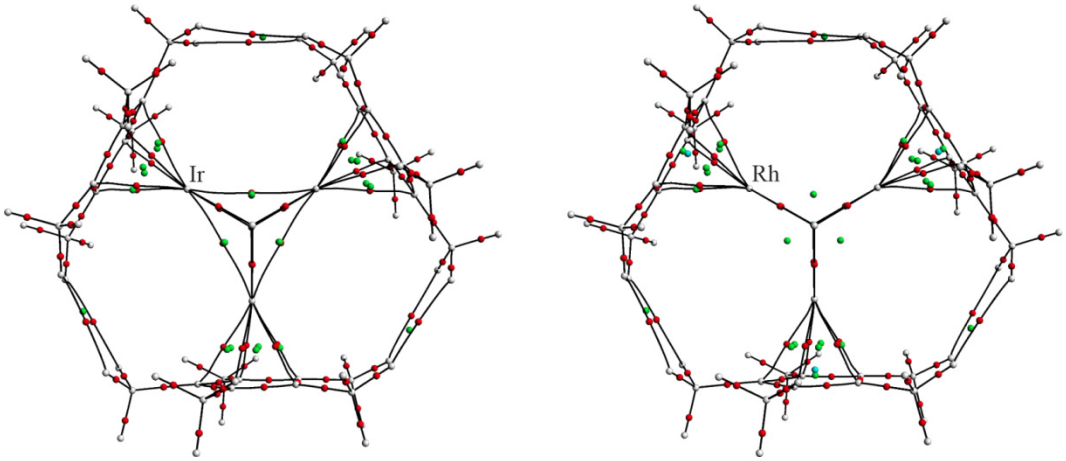

Fig. 1. Electron density critical points and bond pathways in $[Cp^*_3M_3Se_2]^{2+}$ cations where M = Rh, Ir for the PBE-D3(BJ) functional.

annihilate. The properties of critical points (Table 1) show that all metal–ligand bonds have the intermediate character, which is typical. The Ir–Ir bonds belong to the same intermediate type. The properties of Ir–Ir–Se ring points are very similar to the Ir–Ir bcp properties. Consequently, the conclusion can be drawn that in this spatial region, the electron density changes slowly, which is consistent with the instability of these points relative to different exchange-correlation functionals. The metallicity [20] of Ir–Ir bonds indicates that they adopt a partially metallic character, however, they are closer to nonmetallic bonds (metallic bonds correspond to $\xi_m > 25$; nonmetallic bonds correspond to $\xi_m < 5$). Thus, Ir–Ir bcp are most likely to be a geometric artifact, and it seems better to assign them to multicenter Ir–Se–Ir–Se bonds rather than Ir–Ir bonds. It is also worth noting that the unusual electron localization, which was proposed to interpret as a multicenter bond in [2], is present in both cations (Fig. S3, Supplementary Materials).

Localized orbitals. Since the canonical Kohn–Sham orbitals of the complexes under study are strongly delocalized, they are inconvenient to analyze the bonding (Fig. S1, Supplementary Materials), therefore, we considered the localized orbitals. The analysis was carried out for calculations performed with the PBE-D3(BJ) functional because it gave the

TABLE 1. Properties of Some Electron Density Critical Points in $[Cp^*_3M_3Se_2]^{2+}$ Cations for the Calculation with the PBE-D3(BJ) Functional. The Values are Averaged Over the Equivalent Points. $D_{A–B}$ is the Distance Between the Respective Atoms, $\rho(\mathbf{r}_{BCP})$ is the Electron Density, $\Delta\rho(\mathbf{r}_{BCP})$ is the Laplacian of Electron Density, $V(\mathbf{r}_{BCP})$ is the Potential Energy Density, $G(\mathbf{r}_{BCP})$ is the Kinetic Energy Density, ξ_m is the Metallicity [20]

Bond	$D_{A–B}$, Å	$\rho(\mathbf{r}_{BCP})$, au	$\Delta\rho(\mathbf{r}_{BCP})$, au	$V(\mathbf{r}_{BCP})$, au	$G(\mathbf{r}_{BCP})$, au	ξ_m, au
			$[Cp^*_3Rh_3Se_2]^{2+}$			
BCP(Rh–Se)	2.409	0.0874	0.1222	–0.1090	0.0698	9.6964
BCP(Rh–C)	2.199	0.0863	0.2093	–0.1143	0.0833	5.5549
RCP(Rh–Se–Rh–Se)	–	0.0431	0.0730	–0.0365	0.0274	4.9949
CCP(Rh–Rh–Rh–Se–Se)	–	0.0357	0.0927	–0.0299	0.0266	2.8725
			$[Cp^*_3Ir_3Se_2]^{2+}$			
BCP(Ir–Se)	2.422	0.0943	0.1046	–0.1209	0.0735	12.8739
BCP(Ir–C)	2.205	0.0945	0.1936	–0.1287	0.0886	6.9833
BCP(Ir–Ir)	2.884	0.0518	0.0690	–0.0471	0.0322	7.1868
RCP(Ir–Ir–Se)	–	0.0516	0.0734	–0.0472	0.0328	6.7176
CCP(Ir–Ir–Ir–Se–Se)	–	0.0396	0.1103	–0.0357	0.0316	2.8792

geometry closest to the experimental one. There are different ways to transform the canonical delocalized molecular orbitals into localized ones. One of the most popular methods of this kind is the Boys–Foster method [7] consisting in minimizing the spatial extension of each orbital. The analysis of Boys–Foster orbitals of the cations being studied revealed differences between similar Rh and Ir complexes (Fig. 2). Since the lone pairs on both Se and the Se–*M* bond are very similar, the rhodium complex contains three-center Rh–Rh–Se orbitals while the Ir complex contains four-center Ir–Se–Ir–Se orbitals.

NBO. According to the NBO analysis data, electrons are strongly delocalized in both cations. The contribution of non-Lewis orbitals is 13.88 *e* for the rhodium cation and 11.49 *e* for the iridium one, which is much larger than that in $[Cp^*M(SnCl_3)_nCl_{3-n}]^-$ (*M* = Rh, Ir) [21] and *cis*-$[X1X2Rh(CO)_2]^-$ (*X*1, *X*2 = Cl, Br, I) [22] anionic complexes. The high electron delocalization is due not only to the presence of three Cp* rings but also the strong delocalization in the $\{M_3Se_2\}^{2+}$ cluster core (Table 2). An increase in the electron delocalization in the rhodium cation compared to the iridium cation is explained by a higher population of antibonding *M*–Se orbitals.

The NBO analysis detects three lone pairs on Ir, which correspond to 5*d* orbitals, and two lone pairs on Rh, which correspond to 4*d* orbitals, and one partially occupied lone vacancy (LV) on Rh corresponding to the 5*s* orbital. Lone pairs on Se have the same composition in both cations (~75% of the 4*s* orbital and ~25% of the 4*p* orbital) whereas the *M*–Se bonds are composed differently (Fig. 3, Table 3). In the iridium cation, selenium greatly contributes to the bond orbital. Moreover,

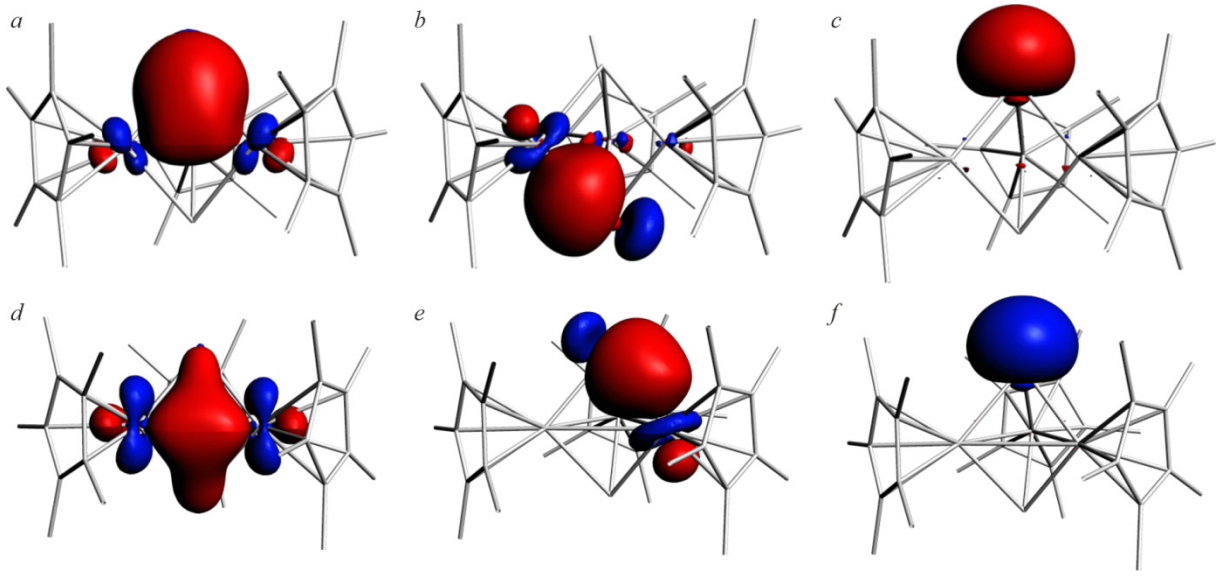

Fig. 2. Some Boys–Foster localized orbitals in $[Cp^*_3M_3Se_2]^{2+}$ cations. For *M* = Rh: Rh–Se–Rh bond (*a*), Rh–Se bond (*b*), lone pair on Se (*c*). For *M* = Ir: Ir–Se–Ir–Se bond (*d*), Ir–Se bond (*e*), lone pair on Se (*f*).

TABLE 2. Population of Different Types of Non-Lewis NBOs

Bond	Rh	Ir
LV (C)	2.77	2.79
BD* (C–C)	0.87	0.90
BD* (C–H)	0.39	0.39
3C(*M*–C–C)	–	2.57
3C*(*M*–C–C)	–	1.47
BD* (*M*–C)	2.52	–
LV (*M*)	1.22	–
BD* (*M*–Se)	5.40	2.65
All RY	0.71	0.71

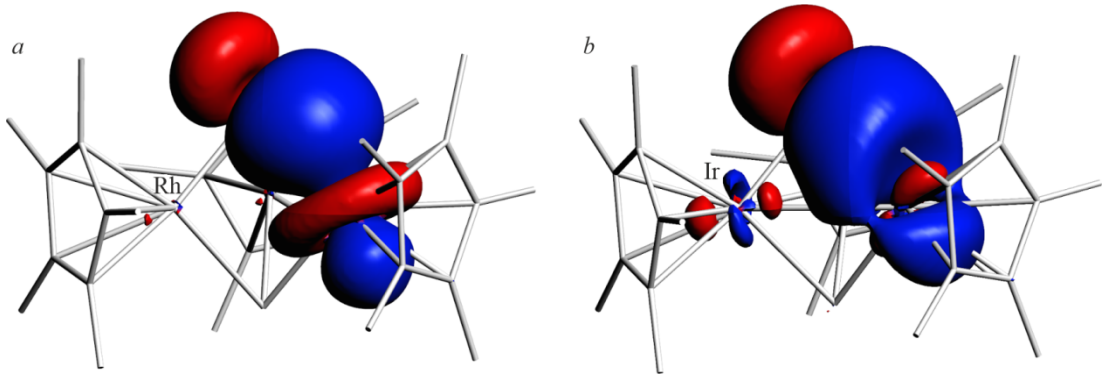

Fig. 3. NBO bond orbital (BD (*M*–Se)) in rhodium (*a*) and iridium (*b*) cations.

TABLE 3. Composition of NBOs Corresponding to the Metal–Selenium Bond

BD(Rh–Se)	(59.92%) Rh *s*(2.19%) *p*(0.07%) *d*(97.73%) *f*(0.01%)
	(40.08%) Se *s*(8.60%) *p*(90.84%) *d*(0.54%) *f*(0.02%)
BD(Ir–Se)	(35.30%) Ir *s*(48.10%) *p*(0.17%) *d* (51.70%) *f*(0.04%)
	(64.70%) Se *s*(8.31%) *p*(91.08%) *d* (0.59%) *f*(0.02%)

the iridium contribution contains 48% of the valence 6*s* orbital, while in the rhodium cation, the contribution of the 5*s* orbital is only 2% in the Rh–Se bond. Distinctions are also observed in *M*–Cp* bonds. For the rhodium complex NBO shows two-center Rh–C bonds and three-center Ir–C–C bonds for the iridium complex (Fig. S2, Supplementary Materials).

Calculation of NMR parameters. The calculated NMR parameters for the cations under study are well consistent with the known experimental data (Table 4) and are even more accurate than those obtained in earlier works [2, 3]. The reason for this can be either the improved geometry of the cations or the taking into account of relativistic effects at the spin-orbit level rather than only scalar one in these calculations of NMR parameters.

The electron shielding of nuclei in the magnetic field is usually divided into three components: diamagnetic (mainly determined by core electrons of the atom), paramagnetic (arising mainly due to valence electrons), and relativistic spin-orbit contribution. The major part of the difference in Se shielding in the Rh and Ir cations is associated with a change in the paramagnetic contribution (Table 5), which indicates differences in the properties of chemical bonds around the selenium

TABLE 4. Calculated and Experimental NMR Shifts (ppm) for $[Cp^*_3M_3Se_2]^{2+}$ Cations

Chemical Shift	Rh		Ir	
	Calculation	Experiment [2]	Calculation	Experiment [3]
$\delta(^{77}Se)$	1747.2	1685	897.3	944
$\delta(^{13}C)$	11.6; 114.1	–	11.3; 107.4	11.0; 98.1
$\delta(^{1}H)$	2.09	2.02	2.41	2.31

TABLE 5. Different Contributions to the Shielding of ^{77}Se Nuclei in $[Cp^*_3M_3Se_2]^{2+}$ Cations (ppm)

Diamagnetic		Paramagnetic		Spin-orbit	
Rh	IIr r	Rh	Ir	Rh	Ir
3003.4	2997.8	–3262.8	–2484.4	231.9	309.1
Difference					
5.6		–778.4		–77.2	

TABLE 6. Contributions of Different Elements of the Electronic Structures (NBO) of $[Cp^*_3M_3Se_2]^{2+}$ Cations to the Sum of Paramagnetic and Spin-Orbit Parts of ^{77}Se Shielding (ppm.)

M = Rh		M = Ir	
∑ CR(Se)	–2.1	∑ CR(Se)	69.5
LP(Se)	–409.2	LP(Se)	–137.2
∑ BD(Rh–Se)	–1474.7	∑ BD(Ir–Se)	–1496.9
		∑ BD(Ir–Se′)	–50.9
∑ BD*(Rh–Se)	–1246.0	∑ BD*(Ir–Se)	–482.0
∑ LP(Rh)	–59.0	∑ LP(Ir)	–86.4
∑ LV(Rh)	245.5	∑ RY(Ir)	–74.3
∑ RY(Se)	–157.3	∑ RY(Se)	112.2
		∑ RY(Se′)	14.5

atom. The difference in the spin-orbit contribution seems to arise because of the Rh replacement by heavier Ir. It is of the same order of magnitude as in the change of ^{119}Sn shielding in Rh and Ir complex anions [21].

Analysis of ^{77}Se shielding. It is possible to distinguish the contributions of different NBOs to ^{77}Se shielding (Table 6). It should be mentioned that NBOs are determined for the wave function calculated with taking into account only scalar relativistic effects. Then the two-component wave function was expanded in terms of these scalar NBOs.

When rhodium is substituted by iridium, substantial changes occur in contributions of the Se lone pair and antibonding *M*–Se orbitals. In the case of iridium, contributions of orbitals of the second selenium atoms also appear. This is consistent with Boys–Foster orbitals indicating four-center Ir–Se–Ir–Se interactions for Ir. LV on Rh gives the shielding contribution, which slightly compensates for a decrease in shielding from other elements of the electronic structure in the rhodium complex.

CONCLUSIONS

The electronic structure of the pair of similar $[Cp^*_3M_3Se_2]^{2+}$ (M = Rh, Ir) cations is studied. The AIM analysis of the electron density shows small differences. The Rh–Rh bcp are absent for all exchange-correlation functionals whereas the Ir–Ir bonds are present for the cases where the optimized Ir–Ir distance is less than 2.900 Å. Boys–Foster localized orbitals indicate the presence of three-center Rh–Se–Rh interactions for rhodium and four-center Ir–Se–Ir–Se interactions for iridium. The NBO analysis demonstrates the great electron delocalization in both cations. The Ir–Se bond orbitals have a significantly larger contribution of the iridium valence *s* orbital than Rh–Se bonds.

Contributions of different elements of the electronic structure to the shielding of Se nuclei in the magnetic field are analyzed. The difference in ^{7}Se NMR shifts in $[Cp^*_3M_3Se_2]^{2+}$ cations is due to a change in the contribution of the lone pair on Se, antibonding *M*–Se orbitals, and the admixture of orbitals of the second Se atom in the iridium complex.

FUNDING

The authors acknowledge the support of the Ministry of Science and Higher Education of the Russian Federation (project No. 121031700313-8).

CONFLICT OF INTERESTS

The author declares that he has no conflicts of interests.

REFERENCES

1. M. Fedotov. NMR in Inorganic and Coordination Chemistry. Cambridge, England: Cambridge International Science, **2013**.
2. P. A. Abramov, M. N. Sokolov, I. V. Mirzaeva, and N. K. Moroz. Synthesis, NMR and quantum chemical studies of the $[Cp_3Rh_3Se_2]^{2+}$ clusters ($Cp = \eta^5$-C_5Me_5, η^5-C_5Me_4Et, η^5-$C_5H_3{}^tBu_2$). *Russ J. Coord. Chem.*, **2013**, *39*(5), 379. https://doi.org/10.1134/S1070328413050011
3. P. A. Abramov, N. F. Zakharchuk, A. V. Virovets, I. V. Mirzaeva, and M. N. Sokolov. Hydrogen selenide in M–Se and C–Se bond formation. $[Cp^*_3Ir_3Se_2]^{2+}$ clusters: New synthesis, molecular and electronic structure and related studies. *J. Organomet. Chem.*, **2014**, *767*, 65. https://doi.org/10.1016/j.jorganchem.2014.05.034
4. A. D. Becke. Density-functional exchange-energy approximation with correct asymptotic behavior. *Phys. Rev. A*, **1988**, *38*, 3098. https://doi.org/10.1103/PhysRevA.38.3098
5. J. P. Perdew. Density-functional approximation for the correlation energy of the inhomogeneous electron gas. *Phys. Rev. B*, **1986**, *33*, 8822. https://doi.org/10.1103/PhysRevB.33.8822
6. R. F. W. Bader. Atoms in Molecules: a Quantum Theory. New York, USA: Oxford University Press, **1990**. https://doi.org/10.1134/S0022476622100122
7. S. F. Boys. Construction of molecular orbitals to be minimally variant for changes from one molecule to another. *Rev. Mod. Phys.*, **1960**, *32*(2), 296. https://doi.org/10.1103/RevModPhys.32.300.
8. S. Deeken, G. Motz, V. Bezugly, H. Borrmann, F. R. Wagner, and R. Kempe. Metal–metal bonding in sterically frustrated dipalladium species. *Inorg. Chem.*, **2006**, *45*(23), 9160. https://doi.org/10.1021/ic0610987
9. E. D. Glendening, J. K. Badenhoop, A. E. Reed, J. E. Carpenter, J. A. Bohmann, C. M. Morales, C. R. Landis, and F. Weinhold. NBO 6.0. Madison, Wisconsin, USA: Theoretical Chemistry Institute, University of Wisconsin, **2013**, https://nbo6.chem.wisc.edu/.
10. J. A. Bohmann, F. Weinhold, and T. C. Farrar. Natural chemical shielding analysis of nuclear magnetic resonance shielding tensors from gauge-including atomic orbital calculations. *J. Chem. Phys.*, **1997**, *107*(4), 1173. https://doi.org/10.1063/1.474464
11. J. Autschbach. Analyzing NMR shielding tensors calculated with two-component relativistic methods using spin-free localized molecular orbitals. *J. Chem. Phys.*, **2008**, *128*(16), 164112. https://doi.org/10.1063/1.2905235
12. ADF 2017. Amsterdam, The Netherlands: SCM, Vrije Universiteit, Theoretical Chemistry, **2017**, http://www.scm.com.
13. E. Van Lenthe and E. J. Baerends. Optimized Slater-type basis sets for the elements 1-118. *J. Comput. Chem.*, **2003**, *24*, 1142. https://doi.org/10.1002/jcc.10255
14. E. van Lenthe, R. van Leeuwen, E. J. Baerends, and J. G. Snijders. Relativistic regular two-component Hamiltonians. *Int. J. Quantum Chem.*, **1996**, *57*, 281. https://doi.org/10.1002/(SICI)1097-461X(1996)57:3<281::AID-QUA2>3.0.CO;2-U
15. G. Schreckenbach and T. Ziegler. The calculation of NMR shielding tensors using GIAO′s and modern density functional theory. *J. Phys. Chem.*, **1995**, *99*, 606. https://doi.org/10.1021/j100002a024
16. M. Swart, A. W. Ehlers, and K. Lammertsma. Performance of the OPBE exchange-correlation functional. *Mol. Phys.*, **2004**, *102*, 2467. https://doi.org/10.1080/00268970420002750l7
17. C. Lee, W. Yang, and R. G. Parr. Development of the Colle–Salvetti correlation-energy formula into a functional of the electron density. *Phys. Rev. B*, **1988**, *37*, 785. https://doi.org/10.1103/PhysRevB.37.785
18. M. Swart. A new family of hybrid density functionals. *Chem. Phys. Lett.*, **2013**, *580*, 166. https://doi.org/10.1016/j.cplett.2013.06.045
19. S. Grimme, S. Ehrlich, and L. Goerigk. Effect of the damping function in dispersion corrected density functional theory. *J. Comput. Chem.*, **2011**, *32*, 1457. https://doi.org/10.1002/jcc.21759

20. P. W. Ayers and S. Jenkins. Bond metallicity measures. *Comput. Theor. Chem.*, **2015**, *1053*, 112. https://doi.org/10.1016/j.comptc.2014.10.040
21. I. V. Mirzaeva. Large relativistic effects in ^{119}Sn NMR parameters: A case study of complex anions $[Cp^*M(SnCl_3)_nCl_{3-n}]^-$, where M = Rh, Ir; n = 1, 2, 3. *Comput. Theor. Chem.*, **2021**, *1205*, 113432. https://doi.org/10.1016/j.comptc.2021.113432
22. I. V. Mirzaeva and S. G. Kozlova. The nature of halogen dependence of ^{103}Rh NMR chemical shift in complex anions *cis*-$[X1X2Rh(CO)_2]^-$ (X1, X2 = Cl, Br, I). *J. Struct. Chem.*, **2019**, *60*(11), 1750. https://doi.org/10.1134/S0022476619110076